

# Gold nanorods 3D-supercrystals as surface enhanced Raman scattering spectroscopy substrates for the rapid detection of scrambled prions

Ramón A. Alvarez-Puebla<sup>a,1</sup>, Ashish Agarwal<sup>b</sup>, Pramit Manna<sup>c</sup>, Bishnu P. Khanal<sup>c</sup>, Paula Aldeanueva-Potel<sup>a</sup>, Enrique Carbó-Argibay<sup>a</sup>, Nicolas Pazos-Pérez<sup>a</sup>, Leonid Vigderman<sup>c</sup>, Eugene R. Zubarev<sup>c,1</sup>, Nicholas A. Kotov<sup>a,b,1</sup>, and Luis M. Liz-Marzán<sup>a,1</sup>

<sup>a</sup>Departamento de Química-Física and Unidad Asociada Consejo Superior de Investigaciones Científicas–Universidade de Vigo, 36310 Vigo, Spain;

<sup>b</sup>Departments of Chemical Engineering, Materials Science and Engineering, and Biomedical Engineering, University of Michigan, Ann Arbor, MI 48109; and <sup>c</sup>Department of Chemistry, Rice University, Houston, TX 77005

Edited by Nicholas J. Turro, Columbia University, New York, NY, and approved March 28, 2011 (received for review November 4, 2010)

**Highly organized supercrystals of Au nanorods with plasmonic antennae enhancement of electrical field have made possible fast direct detection of prions in complex biological media such as serum and blood. The nearly perfect three-dimensional organization of nanorods render these systems excellent surface enhanced Raman scattering spectroscopy substrates with uniform electric field enhancement, leading to reproducibly high enhancement factor in the desirable spectral range.**

**S**urface enhanced Raman scattering (SERS) spectroscopy is not only one of the most sensitive analytical techniques but also can be used under biological conditions. Additionally, SERS signals are strongly dependent on conformational changes in macromolecules such as proteins (1). Unfortunately, although SERS of proteins has been consistently investigated during the last decade (2–6), enhancement factors (EFs) obtained for most conventional (nonfluorescent) proteins are still insufficient for their direct detection in complex biological media (7). There are two additional very serious challenges as well. Both quantitative detection by SERS and reproducible geometry of the “hot spots” necessary for SERS are difficult to achieve. The way to solve these challenges is to design and fabricate a highly organized photonic structure (8) that provides a high electromagnetic field enhancement in a reproducible geometry (9, 10). Recent demonstration of near-field focalization by nanoantennas (11, 12) has paved the way for development of ultrasensitive SERS substrates that can concentrate the near field within certain confined regions, allowing one to obtain extremely high EFs (13–15). Such a nanoantenna effect was predicted and found for nanorod (NR) dimers, where the maximum focalization is present at the NR tips (16, 17). One can hypothesize, therefore, that a highly organized system of NRs (18–21) acting as an extended nanoantenna may provide resolution for the SERS challenges of proteins or their segments. In turn, this hypothesis can lead to significant technological development for relevant biomedical problems. One example of those problems is the presymptomatic detection of scrambled prions directly in biological fluids.

Prions are hard-to-detect infectious agents that cause a number of fatal neurodegenerative diseases in mammals such as bovine spongiform encephalopathy (BSE), scrapie of sheep, and Creutzfeldt–Jakob disease (CJD) of humans (22), and recently traced as well to other neurodegenerative syndromes as Alzheimer’s (23) and Parkinson (24). Invariably, all of these diseases involve the modification of the endogenous and functional prion protein (PrP<sup>C</sup>) into a nonfunctional but much more stable form (PrP<sup>Sc</sup>) giving rise to the so-called amyloid plaques in the brain and other nervous tissues (25). Detection of its presence for contention in cattle or diagnosis in humans or blood transfusion banks (26) is very difficult even by state-of-the-art immunological methods such as fluorescence immunoassay, RIA, or ELISA (27) or protein misfolding cyclic amplification (PMCA), which can be

used for presymptomatic prion detection. However, it is complex and requires more than 525 h per sample (7 cycles of 75 h each) (27, 28). Thus the confirmation of BSE, scrapie, or CJD still relies on the postmortem imaging analysis of the degenerated tissues of the suspected individuals, usually resulting in late response, implying risk of pandemic outbreak with additional important economic consequences. The development of unique detection techniques capable of accurately detecting/diagnosing the presence of prions in the blood or serum of infected but not clinically sick animals to avoid the dissemination of the disease is therefore much needed.

## Results and Discussion

Gold NRs (75 × 25 nm; aspect ratio 3) were made using the seed-mediated method (9, 29). Modifications of the synthetic protocol described in *Materials and Methods* resulted in improvements of the resulting NRs, which are quite significant: (i) a 1,000-fold increase in the amount of NRs synthesized in one batch and (ii) very narrow size distributions ( $\sigma \sim 3\%$ ). Consequently, NRs were able to spontaneously and reproducibly crystallize into 3D colloidal crystals (supercrystals) arranged as individual islands of fairly uniform dimensions (Fig. 1A) when the aqueous NR dispersions were slowly dried in humid atmosphere (Fig. 1). Both the diameter (Fig. 1B) and height of individual NR islands were in the range of 1  $\mu$ m, which corresponds to approximately 15 layers of NRs perpendicular to the substrate. SEM examination revealed that the crystalline assemblies do not contain any grain boundaries and the orientational and positional order of individual NRs is the same throughout the entire structure and from island to island. The separation between the adjacent NRs is approximately 3 nm, which corresponds to a bilayer of the cationic surfactant cetyltrimethylammonium bromide (CTAB), and has been described as the optimal separation between particles for the generation of hot spots (30–32).

The optical response of the supercrystals (Fig. 2D) was characterized using an inverted dark-field microscope. The localized surface plasmon resonance was found to be very homogeneous throughout the entire surface and exhibits a maximum at 696 nm. Electric near-field enhancement simulations of different NR supercrystals support the hypothesis of the nanoantenna effect. Comparison of the simulations for a three-layer rod-stacked

Author contributions: R.A.A.-P., E.R.Z., N.A.K., and L.M.L.-M. designed research; R.A.A.-P., A.A., P.M., B.P.K., P.A.-P., E.C.-A., N.P.-P., and L.V. performed research; R.A.A.-P. analyzed data; and R.A.A.-P., E.R.Z., N.A.K., and L.M.L.-M. wrote the paper.

The authors declare no conflict of interest.

This article is a PNAS Direct Submission.

<sup>1</sup>To whom correspondence may be addressed. E-mail: ramon.alvarez@uvigo.es, lmarzan@uvigo.es, kotov@umich.edu, or zubarev@rice.edu.

This article contains supporting information online at [www.pnas.org/lookup/suppl/doi:10.1073/pnas.1016530108/-DCSupplemental](http://www.pnas.org/lookup/suppl/doi:10.1073/pnas.1016530108/-DCSupplemental).

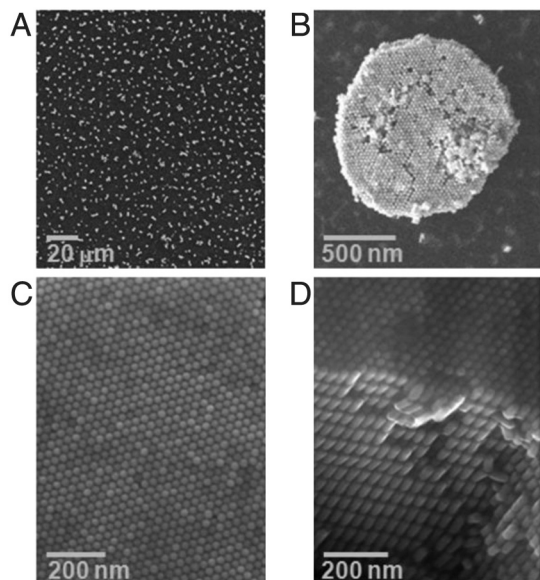


**Fig. 1.** Nanorod supercrystals morphology. (A–C) SEM images corresponding to different magnifications of a typical nanorod supercrystal island film. (D) View from the edge of the supercrystal.

supercrystal (Fig. 2E) and a single rod monolayer (Fig. 2F) indicate increased plasmon concentration on the top surface as layers of rods are added. Note that the field intensity between the rods in the middle of the stack is also very high (see [Supporting Information](#)). The island morphology of the NR film with tall columns of supercrystals (Fig. 1A and B) helps taking advantage of the interstitial hot spots accessible for analytes from the solution

as well. Characterization of the SERS enhancing efficiency of NR supercrystals was carried out in the same area, using benzenethiol (BT). A highly homogeneous intensity was registered for three different laser lines with an extremely high intensity for all of them, which is again consistent with the electric field calculations as shown in the [Supporting Information](#). Extensive comparative testing revealed that NR supercrystals as SERS substrates were largely superior to previously used arrangements of nanoparticles and NRs, including single particle and fractally aggregated or parallel NRs (33) (Fig. 2K and [Supporting Information](#)). Islands of NR supercrystals offer additional advantages for bioanalysis such as chemical stability, reproducibility, and highly homogeneous distribution of field intensity making possible quantitative SERS detection of complex biomolecules. Mechanical robustness of the NR supercrystal islands, which allows multiple use of the substrates upon plasma etching of the previous analyte, is also a plus. It can be exemplified by SERS analysis of BT and a second molecular probe (1-naphthalenethiol, 1NAT) on the same NR supercrystal upon plasma etching of BT (Fig. 3). Notably, after cleaning, no signal of BT was registered (see [Supporting Information](#)) even when mapping a large area ( $30 \times 30 \mu\text{m}$ ) while the morphology of the supercrystal remained unaltered and the SERS intensity was still extremely high.

The unique potential of these SERS substrates was thus exploited for the ultrasensitive detection of scrambled prions within complex biological media such as serum. Due to the high requirement of a biosecurity lab level 3 for manipulation of real prions, we selected a model peptide (106–126, Fig. 4A), widely used to investigate prion diseases (34) as it forms fibrils in vitro and causes apoptotic cell death in neuron culture. First, we investigated the SERS spectra of the biologically active and the scrambled prion in PBS. Then we studied the lower proportion of PrP<sup>Sc</sup> in PrP<sup>C</sup> that can be unambiguously determined. Because

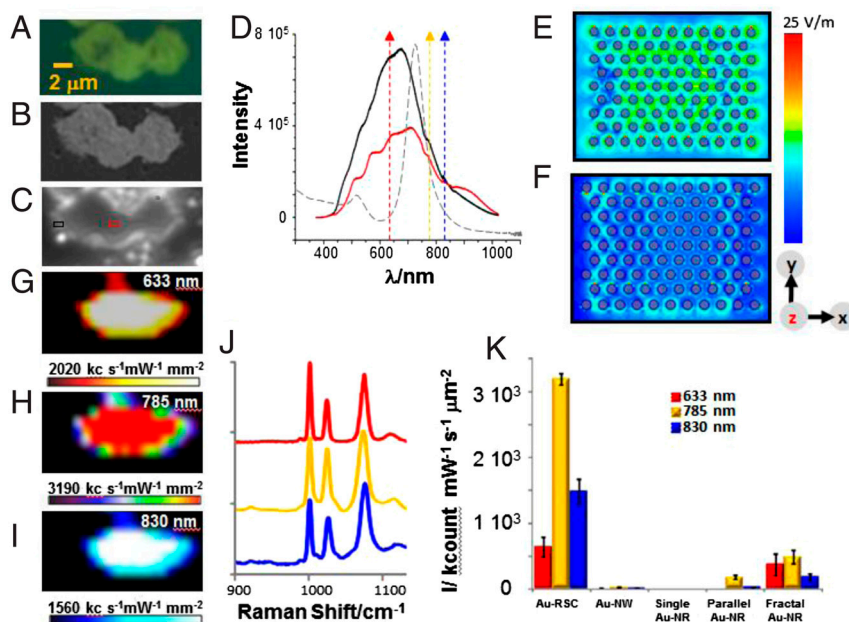


**Fig. 2.** Optical properties of the nanorod supercrystals. (A–C) Optical, SEM, and dark-field images of an NR supercrystal, respectively, after plasma-etching removal of surfactant coating of the NRs. (D) Localized surface plasmon resonance bands of the rods in solution (gray) and within a supercrystal, either at the center or at the edges (red and black boxes of Fig. 2C, respectively). Dotted arrows indicate the excitation laser lines used for SERS. (E and F) Electric field enhancement maps calculated for the top part of a three layer rod-stacked supercrystal (E) and for the same location in a single monolayer (F). (G–J) SERS intensity maps at  $1,072 \text{ cm}^{-1}$  (BT ring breathing) corresponding to the supercrystal in A, for BT as excited with a 633 (G), 785 (H), and 830 nm (I) laser lines, representative SERS spectra for each laser being presented in J. (K) Comparison of the SERS intensities at  $1,072 \text{ cm}^{-1}$  provided by a gold rod supercrystal (Au-RSC) film with common SERS substrates, including aggregated ultralong nanowires (Au-NW), single rods, parallel and fractally aggregated gold NRs (Single Au-NR, Parallel Au-NR, and Fractal Au-NR, respectively). The intensity is the result of averaging over 50 different randomly distributed spots in the supercrystal and those corresponding to maximum intensity for the rest of substrates. More information about the different substrates can be found in the [Supporting Information](#).

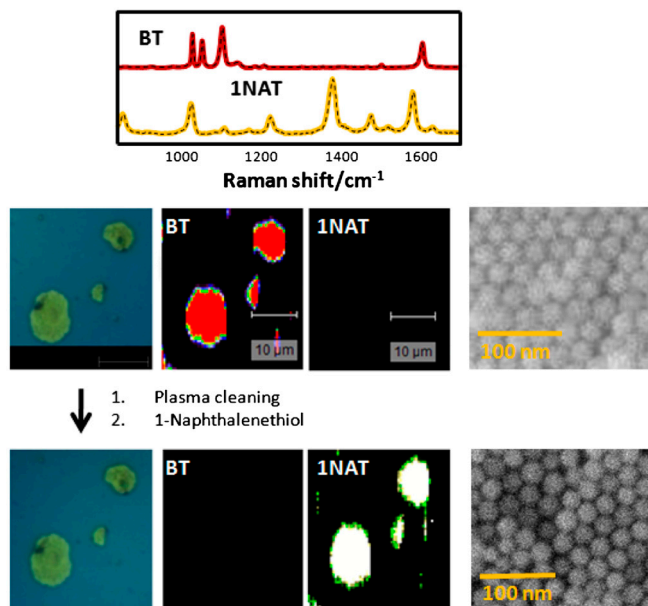


**Fig. 3.** Reusability of supercrystals after plasma cleaning. SEM images and SERS spectra and mapping of a supercrystal before and after cleaning the first analyte ( $1,072\text{ cm}^{-1}$ , BT) and adding a different one ( $1,351\text{ cm}^{-1}$ , 1NAT).

the primary chemical structure of both prions is very similar, so are their respective vibrational patterns (see [Supporting Information](#)). SERS is dominated by a band at  $762\text{ cm}^{-1}$  assigned to the interaction of Au-S-C, and a triplet in PrP<sup>C</sup> ( $1,390$ ;  $1,416$ ; and  $1,446\text{ cm}^{-1}$ ) which becomes a singlet ( $1,448\text{ cm}^{-1}$ ) in the scrambled version. These bands are related to the side-chain bands together with the amide II' and III modes, especially in the -Met-Lys-His-Met- fragment, responsible for the binding of the peptide to the gold surface. It is important to bear in mind that, when prions are mixed, spectral patterns from the misfolded prions are fully identifiable even when their relative concentration is as low as 1% that of the normal prion. This fact is probably due to induction of the misfolding of the  $\alpha$ -helix structure of the endogenous PrP<sup>C</sup> into the  $\beta$ -sheet of the scrambled version. In fact, it is this behavior that has been previously exploited for the detection of prions by PMCA (35). On the other hand, by systematically diluting the mixture containing 1% PrP<sup>Sc</sup> and 99% PrP<sup>C</sup>, we were able to detect scrambled prion signal for a total prion concentration of as low as  $10^{-10}\text{ M}$ , which is equivalent to 10 molecules per area sampled (i.e., zeptomol regime) (see [Supporting Information](#)). Such high sensitivity may make possible direct and fast detection of prions in real complex biological fluids, such as blood or serum, which was never possible before (36). To demonstrate this statement, detection of a mixture containing 1% of scrambled prions in the functional protein was carried out within a complex matrix, such as bovine serum. SERS spectrum of PrP<sup>Sc</sup>:PrP<sup>C</sup> in serum (Fig. 4E) is dominated by bands corresponding to the C-N stretching ( $1,118\text{ cm}^{-1}$ ), Phe ( $1,003$  and  $1,033\text{ cm}^{-1}$ ), Trp ( $1,011$  and  $1,560\text{ cm}^{-1}$ ), Tyr ( $845\text{ cm}^{-1}$ ), and Cys ( $720\text{ cm}^{-1}$ ). Upon sequential dilution of the prion mixture (1% of PrP<sup>Sc</sup> in 99% of PrP<sup>C</sup>) in serum, the characteristic prion bands can still be clearly recognized down to concentrations as low as  $10^{-10}\text{ M}$ . For all the analyzed samples, no evidence of biologically functional prion was found, implying its conversion into the scrambled version, which is consistent with the results obtained in PBS. The fact that the prion proteins can be clearly identified in serum, e.g., a complex solution containing high concentrations of electrolytes and proteins, such as albumins globins, hormones, antibodies, and many other exogenous substances (drugs and microorganisms), is likely to indicate the high affinity of prions for gold, which is in agreement with the capacity

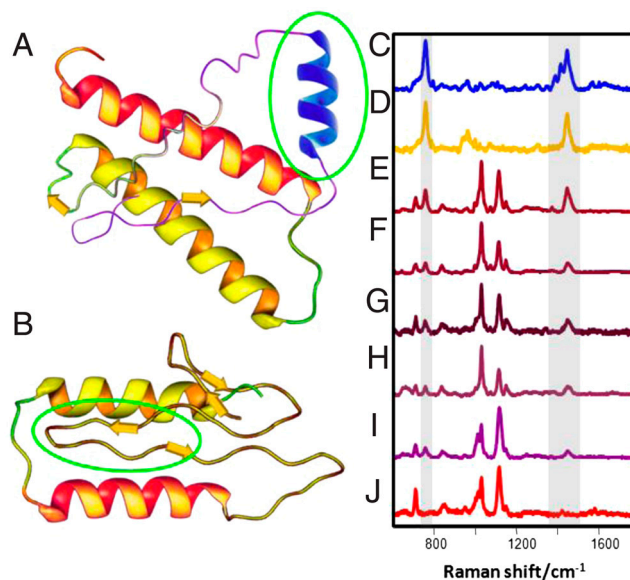


**Fig. 4.** Scheme showing the prion mutation and detection limits for the scrambled version in bovine serum. (A) Biologically active (PrP<sup>C</sup>  $\alpha$ -helix) and (B) scrambled (PrP<sup>Sc</sup>  $\beta$ -sheet) prions; the fragment corresponding to 106–126 peptide is highlighted in green. SERS spectra of (C) PrP<sup>C</sup>  $\alpha$ -helix and (D) PrP<sup>Sc</sup> (scrambled). (E–J) Detection limits of PrP<sup>Sc</sup>:PrP<sup>C</sup> (1:99) in bovine serum at  $10^{-6}$ ,  $10^{-7}$ ,  $10^{-8}$ ,  $10^{-9}$ , and  $10^{-10}\text{ M}$  in total prion, respectively; and (J) bovine serum.

of -Met-Lys-His-Met- groups present in prions to efficiently chelate Au atoms (37). When greater surface area is available, bigger components can interact as well.

Further, to test the viability of this technique to discern contaminated blood samples in, for example, transfusion blood banks (26), and demonstrate validity of a SERS-based protocol for such analysis, an experiment was designed to detect low concentration of prions in human blood. Samples of blood spiked with prions were centrifuged to obtain plasma (serum plus coagulation factors). Fig. 5 shows SERS spectra of blood and plasma before and after addition of prions. Direct analysis of blood (Fig. 5A and B) does not offer any insights about the presence of infection. Notwithstanding, after centrifugation of the sample to obtain plasma, scrambled prions are clearly identified at the attomol regime (Fig. 5C and D). The identification becomes even more

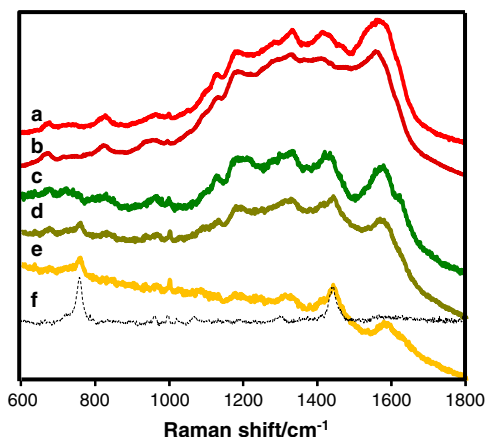


**Fig. 5.** Prion ultradetection in human blood. SERS spectra of (A) natural and (B) spiked human blood; (C) natural and (D) spiked human plasma. (E) SERS spectra spiked human plasma after spectral subtraction of the matrix (human plasma). (F) SERS spectra of the scrambled prion (equivalent to that of Fig. 4B).



obvious after spectral subtraction (Fig. 5E) of the plasma vibrational signature (Fig. 5 C and D).

In summary, highly organized supercrystals of Au NRs with plasmonic antennae enhancement of electrical field have made possible direct detection of prions in complex biological media such as serum or blood. Three-dimensional organization of NRs into supercrystals render these systems excellent SERS substrates with uniform electric field enhancement, high intensity of the hot spots, and reproducible EFs in the desirable spectral range. From the practical perspective, these substrates show great promise for the fast online presymptomatic detection of prions in biological fluids such as blood or urine. This approach also avoids increased risk of infection or additional digestion stages, which further increase the time for detection and uncertainty of the final results.

## Materials and Methods

**Materials.** Tetrachloroauric acid, silver nitrate, sodium borohydride, ascorbic acid, trisodium citrate, hydrochloric acid, CTAB, oleylamine (OA, technical grade, 70%), chloroform (99%), ethanol (EtOH), BT, serum albumin, PBS solution, prion protein fragment 106–126 (PrP<sup>C</sup>), prion protein fragment 106–126 scrambled (PrP<sup>Sc</sup>), BSA, bovine serum, and human blood were purchased from Sigma-Aldrich. Naphthalene-1-thiol (1NAT) was obtained from Acros Organics. All chemicals were used as received. All glassware was washed with *aqua regia* prior to the experiments. Milli-Q deionized water (resistivity > 18 MΩ cm<sup>-1</sup>) was used for all preparations.

**Synthesis of Monodisperse NRs and Supercrystals.** Au NRs were prepared by a modification of the usual seeded-growth method (38). Specifically, the growth solution was prepared by a twofold increase in the concentration of Au (III) ions, AgNO<sub>3</sub>, and ascorbic acid, whereas the amount of seed particles solution was increased from 12 μL to 9.6 mL as compared with the conventional method (see below). The presence of a slight excess of ascorbic acid (0.1 mol equiv with respect to gold) promotes the growth of NRs as soon as the seed solution is added. The NRs reach the size of 45 nm in length and 10 nm in width within 2 h, at which point the growth stops, although there is still nearly 80% of the initial gold chloride present in solution. All these ions can be reduced and deposited onto the surface of the NRs if an additional amount of ascorbic acid (1.1 mol equiv) is introduced at a very slow rate. This process leads to an amplification of the NRs dimensions, which reach 75 nm in length and 25 nm in diameter. Most importantly, the size distribution of NRs becomes much narrower ( $\sigma \sim 3\%$ ) as shown in the [Supporting Information](#). Because of their narrow size distribution, the NRs have sharp peaks in the UV-visible absorption spectrum and (see [Supporting Information](#)) can crystallize into 3D colloidal crystals when a drop of their aqueous suspension is cast on a substrate and allowed to dry very slowly (24 h) in a saturated moist atmosphere.

**Preparation of Flexible Gold Ultralong Nanowire Films for Comparison of SERS Effects.** In a typical synthesis, HAuCl<sub>4</sub> (2.60 mg) was dissolved in OA (5 mL) by vortexing the mixture at room temperature until the solution turned from pale yellow, the characteristic color of OA, to an intense orange color, which indicates complex formation between Au<sup>3+</sup> and OA. Thereafter, the solution was left undisturbed for 24 h, during which time the solution color changed again gradually from orange to pale yellow, indicating the reduction of Au<sup>3+</sup> to Au<sup>0</sup>. Next, the gold solution was aged for 5 d in a thermostatic bath at 35 °C. Then, to 1 mL of this solution, 3 mL of CHCl<sub>3</sub> and 3 mL ethanol were added. The solution was centrifuged at 5,000 rpm for 20 min. The supernatant was discarded and the precipitate redispersed in 3 mL CHCl<sub>3</sub>. A second centrifugation step (4,000 rpm, 60 min) was carried out after the addition of ethanol (3 mL), the supernatant was discarded, and the precipitate redispersed in 3 mL CHCl<sub>3</sub> (see [Supporting Information](#)). Films were prepared by drop-casting and air-drying 10 μL of the suspension on an indium tin oxide (ITO) slide.

**Preparation of Gold Nanorod Films.** A solution of gold seeds was prepared by borohydride reduction of HAuCl<sub>4</sub> (0.25 mM, 5 mL) in aqueous CTAB solution (0.1 M). An aliquot of seed solution (24 μL) was added to a growth solution (10 mL) containing CTAB (0.1 M), HAuCl<sub>4</sub> (0.5 mM), ascorbic acid (0.8 mM), silver nitrate (0.12 mM), and HCl (19 mM). For the deposition of the gold nanorods on silicon wafers, 2 mL of the as-prepared suspension was centrifuged twice for 15 min, first at 6,500 rpm and then at 4,000 rpm. After discarding the supernatant, the precipitate was redispersed finally in 1 or 0.25 mL of water, either to obtain nonaggregated particles (see

[Supporting Information](#)) or aggregated films made of rods with predominantly parallel orientation, respectively, by spin-coating 10 μL of the suspension on ITO slides. To prepare the fractal film of nanorods, the as-prepared suspension was centrifuged five times (6,000 rpm, 15 min) and, after discarding the supernatant, 10 μL of the precipitate, redispersed in 0.25 mL of water, was drop-cast on a ITO slide.

**Characterization.** Transmission electron microscopy images were obtained using a transmission electron microscope (JEOL JEM-1010) operating at an acceleration voltage of 100 kV. Solid thin films were characterized using a field emission SEM (JEOL JSM-6700f). Gold nanorod supercrystals were imaged and their scattering spectra acquired using a 100-W halogen lamp illumination source on a Nikon Eclipse TE-2000 inverted optical microscope coupled to a Nikon Dark-Field Condenser (dry, 0.95–0.80 N.A.). The scattered light from selected supercrystal areas was collected with a Nikon Plan Fluor-ELWD 40× (0.60 N.A.) objective and focused onto the entrance slit of a MicroSpec 2150i imaging spectrometer coupled with a thermoelectric-cooled CCD camera (PIXIS 1024B ACTON Princeton Instruments). The light scattered by the supercrystals was recorded in the dark-field microscope with collection times of 20 s. SERS experiments were conducted with a micro-Raman Renishaw InVia Reflex system attached to a Leica microscope, a two-dimensional CCD camera, and an automated stage with 100-nm spatial resolution. The spectrograph used high-resolution gratings (1,200 or 1,800 g mm<sup>-1</sup>) with additional bandpass-filter optics. Several laser excitation energies were employed, including laser lines at 633 (HeNe), 785 (diode), and 830 nm (diode). All measurements were made in confocal mode in backscattering geometry using a 100× (0.90 N.A.) objective, which provides a resolution of 500 nm. SERS maps were collected by using the Renishaw StreamLine accessory with a step size of 500 nm.

**Plasma Cleaning of the Nanostructured Surfaces.** Samples on ITO were cleaned with plasma previously to SEM characterization and SERS analysis. In the case of the supercrystals, samples were cleaned as well after the analyte exposure to check the efficiency in removing the organics and the possibility of reusing the sample. Plasma was generated in a Solarus™ (Model 950) Advanced Plasma Cleaning System under the following conditions: 27.5 sccm (standard cubic centimeters per minute) O<sub>2</sub>, 6.4 sccm H<sub>2</sub>, 70 mTorr and exposition of 2 min.

**SERS Characterization.** In order to characterize the gold crystal rods films, BT was adsorbed in gas phase over the whole surface of the films by casting a drop of BT (0.1 M in ethanol) in a Petri box where the film was also contained. Surfaces were then mapped using the Renishaw StreamLine accessory, taking mapping areas of 25 × 35 μm<sup>2</sup>, with a step size of 0.5 nm (1,440 spectra each) upon excitation with three different laser lines: 633, 785, and 830 nm. Acquisition times were set to 200 ms with power at the sample of 1 mW. For comparison, the same experiments (following the same protocol) were carried out on the rest of the films (i.e., noninteracting AuNRs, AuNRs aggregated parallel to each other, and fractally aggregated AuNRs).

**Reusability of the Supercrystal films.** Material recyclability was tested by exposing the substrate to BT in gas phase, registering (see above), cleaning the sample with the H<sub>2</sub>-O<sub>2</sub> plasma (see above), and casting a dilute solution of 1NAT (10 μL, 10<sup>-4</sup> M). After each exposure, the sample was mapped with the Renishaw StreamLine accessory (55 × 67 μm<sup>2</sup>, 500-nm step size with a total spectra collection of 14,310 points) with the 785-nm laser line in the same conditions as described above. Mapping was carried out in two different spectral windows from 905 to 1,190 cm<sup>-1</sup> characteristic of BT and from 1,670 to 1,580 cm<sup>-1</sup>, characteristic of 1NAT. This procedure was repeated in several samples several times to ensure reproducibility.

**Prion Detection.** Stock solutions of PrP<sup>C</sup> and PrP<sup>Sc</sup> 10<sup>-4</sup> M were prepared in PBS (12 mM NaCl, 0.27 mM KCl, and 1 mM phosphate buffer salts). From these, PrP<sup>Sc</sup> solution was consistently diluted in PrP<sup>C</sup> solution (100%, 50%, 25%, 10%, 1%, and 0% in PrP<sup>Sc</sup>). Then, 10-mL samples of each solution were cast each onto a different supercrystal film and studied with SERS ( $\lambda_{\text{ex}}$ : 785 nm, 10 s, 1 mW of power at the sample). Ten points were collected for each sample to ensure reproducibility. This process was repeated as well on a single crystal film, cleaning it with the plasma after each analysis, with similar results. After setting the detection limit of PrP<sup>Sc</sup> in PrP<sup>C</sup> to 1%, absolute detection limits of PrP<sup>Sc</sup> were determined by diluting the stock solution containing 1% of PrP<sup>Sc</sup> in 99% of PrP<sup>C</sup> until concentrations of 10<sup>-11</sup> M. SERS spectra were acquired in the same conditions as described above. To probe the viability of this method to be implemented in real samples with no need

**PNAS**

## CHEMISTRY

Innovación, Spain). N.A.K. acknowledges the Spanish Ministerio de Ciencia e Innovación for a research fellowship. This work was funded by the Spanish Ministerio de Ciencia e Innovación (MAT2010-15374 and MAT2008-05755) and the Xunta de Galicia (PGIDIT09TMT011314PR and 08TMT008314PR). N.A.K. is thankful for research grants from the National Science Foundation (NSF) (R8112-G1, ECS-0601345, 0932823), National Institutes of Health (1R21CA121841 and 5R01EB007350), and Defense Advanced Research Planning Agency (W31P4Q-08-C-0426). Support for E.R.Z. was provided by The Robert A. Welch Foundation (C-1703), NSF (DMR-0547399), and Alliance for Nanohealth (W8XWH-07-2-0101).

- Alvarez-Puebla et al.